

## Single electron transfer in thermally annealed nanoparticle dropcast thick films

Sulolit Pradhan, Xiongwu Kang, Ernesto Mendoza, and Shaowei Chen<sup>a)</sup>

Department of Chemistry and Biochemistry, University of California, 1156 High Street, Santa Cruz, California 95064, USA

(Received 18 November 2008; accepted 8 January 2009; published online 30 January 2009)

A very simple and effective procedure based on thermal annealing was reported in inducing discrete charge transfer in nanoparticle solid films. The particle ensembles were prepared by dropcasting a particle solution onto an interdigitated array electrode. The as-prepared particle films exhibited only linear featureless current-potential profiles in conductivity measurements, whereas after thermal annealing, well-defined staircase features of single electron transfer started to emerge at temperatures higher than 300 K. This was accounted for by the combined consequence of structural rearrangements of nanoparticle cores within the organic protecting matrix and thermal activation of interparticle charge transport. © 2009 American Institute of Physics. [DOI: 10.1063/1.3076132]

Because of their nanocomposite nature, monolayer-protected nanoparticles exhibit unique charge-transfer properties that may be readily manipulated by both the nanoparticle structures as well as interparticle arrangements. Among these, one characteristic is the discrete charge transfer phenomenon even at ambient temperature that arises from the (sub)attofarad molecular capacitance ( $C_{\text{MPC}}$ ) of these nanoparticles, as the energetic barrier for a single electron charging ( $e^2/2C_{\text{MPC}}$ ) may be significantly larger than thermal kinetic energy ( $k_B T$ , with  $k_B$  being the Boltzmann's constant). This is the fundamental basis for the development of nanoparticle-based single electron transistors. Thus far, nanoparticle discrete charge transfer has been observed in scanning tunneling spectroscopic studies of individual nanoparticles, which is reflected by the well-known Coulomb staircase phenomenon, as well as in electrochemical investigation of nanoparticles in solution with a series of evenly spaced voltammetric waves.<sup>1</sup> More recently, single electron transfer (SET) across a nanoparticle monolayer film has also been observed in solid-state electronic conductivity study by deliberate manipulation of the nanoparticle structures and interparticle arrangements.<sup>2-4</sup> However, with nanoparticle thick films, particularly particle films that are prepared by dropcasting a concentrated solution onto an electrode surface, the current-potential profiles are typically featureless. This is largely attributed to the rampant structural defects within the particle films that render it difficult to resolve the individual charging step.<sup>5</sup>

In this study, using alkanethiolate-protected gold nanoparticles as the illustrating example, we report a simple and effective procedure based on low-temperature thermal annealing to induce ordered arrangements of the particles within the nanoparticle dropcast films, leading to the appearance of well-defined SET features.

Specifically, 1-octanethiolate-passivated gold (AuC8) nanoparticles were prepared by using the Brust protocol.<sup>6</sup> The particles were then fractionated by using a binary solvent-nonsolvent mixture of toluene and ethanol,<sup>7,8</sup> followed by thermal annealing in toluene at 110 °C for 8 h in

an oil bath to reduce the core size dispersity.<sup>9</sup> The fraction with an average core diameter of 2.0 nm (with a molecular composition of  $\text{Au}_{314}\text{C}_{891}$ )<sup>10</sup> was used for subsequent measurements.

A particle film was then formed by dropcasting a calculated amount (typically 5  $\mu\text{l}$ ) of a particle solution onto an interdigitated array (IDA) electrode (25 pairs of gold fingers of 3 mm  $\times$  5  $\mu\text{m}$   $\times$  5  $\mu\text{m}$ , from ABTECH). The particle concentration was varied from 0.20 to 0.50, 0.75, 1.00, 1.50, and 2.00 mg/ml in toluene. At least 30 min was allowed for solvent evaporation. The number of layers of nanoparticles was estimated by taking into account the film cross-section area and the total amount of nanoparticles. Conductivity measurements were then carried out in vacuum (Cryogenic Equipment, JANIS CO.) with a CHI710 Electrochemical Workstation at different temperatures (LAKESHORE 331 Temperature Controller). Effects of thermal annealing on the nanoparticle film conductivity were then examined by first heating the particle films at a moderately elevated temperature (typically 340–360 K) for 3 h followed by 1 h of cooling.

Figure 1 shows the current-potential ( $I$ - $V$ ) profiles of a AuC8 particle film prepared by dropcasting 5  $\mu\text{l}$  of a 0.5 mg/ml particle solution in toluene onto an IDA surface (estimated to consist of ca. 30 layers of nanoparticles). It can be seen that within the bias voltage of  $\pm 0.8$  V, the  $I$ - $V$  responses are highly linear throughout the entire temperature range of 100–320 K. Such charge transfer characteristics have indeed been observed extensively in previous studies,<sup>11-15</sup> where the Ohmic behaviors are largely accounted for by the structural defects within the particle films that facilitate interparticle charge transfer. Whereas it is generally assumed that the nanoparticle cores are embedded within an organic matrix resulting from the intercalation of the surface protecting layers from neighboring particles, the exact structural details remain elusive. The fact that only featureless  $I$ - $V$  responses are observed suggests that most probably because of the crude preparation method, there exist rampant structural defects within the particle films, which serve as effective charge percolation pathways (as depicted in the figure inset). Very consistent  $I$ - $V$  characteristics were observed when the particle concentration was varied within

<sup>a)</sup> Author to whom correspondence should be addressed. Electronic mail: schen@chemistry.ucsc.edu.

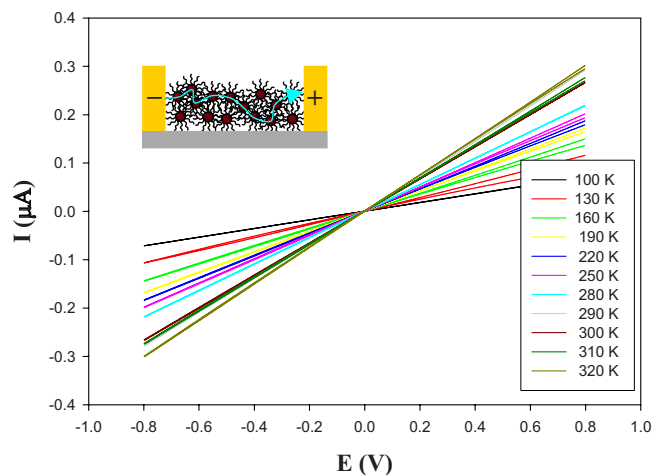


FIG. 1. (Color online)  $I$ - $V$  profiles of an as-prepared dropcast film of AuC8 nanoparticles at different temperatures which were shown as figure legends. The particle film was prepared by spreading  $5\ \mu\text{l}$  of a particle solution ( $0.5\ \text{mg/ml}$ ) onto an IDA electrode. Potential scan rate  $20\ \text{mV/s}$ . Inset depicts the schematic of an as-prepared nanoparticle film. The blue arrow represents a possible percolation pathway.

the range of  $0.2$ – $2.0\ \text{mg/ml}$  (and the film thickness varied accordingly from approximately 10 to 150 layers of particles).

Upon thermal annealing at low temperatures, however, the nanoparticle films exhibited drastically different  $I$ - $V$  profiles and the results were very reproducible. Figure 2 depicts the  $I$ - $V$  responses of the same AuC8 particle films as in Fig. 1 within the same temperature range of  $100$ – $320\ \text{K}$  as the particle film was subjected to annealing at  $340\ \text{K}$  for 3 h. It can be seen that at low temperatures ( $100$ – $300\ \text{K}$ ), there was virtually no difference of the  $I$ - $V$  profiles as compared to those of the as-prepared particle film (Fig. 1). This is better manifested in the difference spectra in the upper inset to the figure. In contrast, at temperatures higher than  $300\ \text{K}$ , the  $I$ - $V$  profiles started to exhibit very well-defined staircase features (at least four steps), which are attributable to the discrete

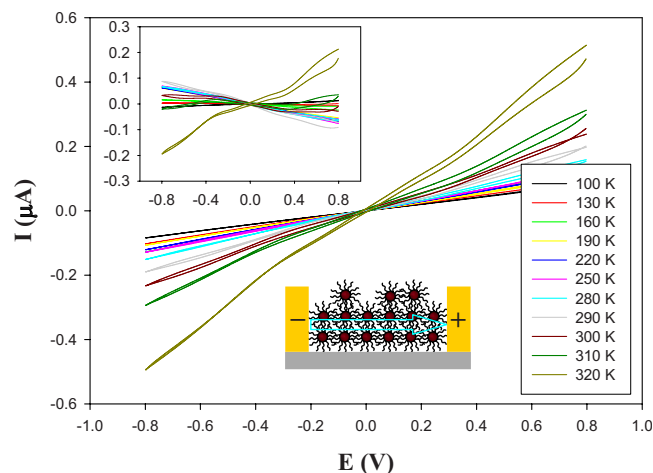


FIG. 2. (Color online)  $I$ - $V$  profiles of the AuC8 particle film at different temperatures (shown as figure legends) after the film had been subjected to thermal annealing at  $340\ \text{K}$  for 3 h. The particle films and all other experimental conditions are the same as those in Fig. 1. Upper inset depicts the difference  $I$ - $V$  profiles between those of the thermally annealed and as-prepared AuC8 particle films (Fig. 1) at varied temperatures. Lower inset shows the schematic of the nanoparticle ensemble after thermal annealing. The blue arrow represents a possible electron-transfer pathway.

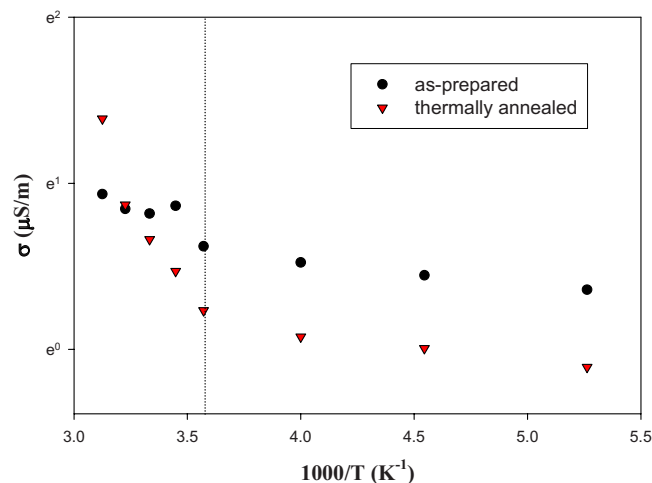


FIG. 3. (Color online) Temperature dependence of the AuC8 particle film conductivity before and after thermal annealing at  $340\ \text{K}$ . Data were obtained by linear regressions of the  $I$ - $V$  curves shown in Figs. 1 and 2.

charge transfer across the nanoparticle films. This behavior is also illustrated in the difference spectra shown in the upper inset. Based on the average potential spacing between adjacent current steps,  $\Delta V = 367\ \text{mV}$ , the effective particle-particle coupling capacitance ( $C_{pp}$ ) may be evaluated to be  $0.44\ \text{aF}$ . Note that a somewhat larger  $C_{pp}$  ( $0.59\ \text{aF}$ ) was observed with Langmuir–Blodgett monolayers of similar gold nanoparticles but with a shorter hexanethiolate protecting layer (AuC6).<sup>3</sup>

We trust that this is the first of its kind with nanoparticle dropcast thick films. Overall, the behaviors are very consistent with previous results of nanoparticle Langmuir–Blodgett monolayers, where SET becomes well defined only at ambient temperature and within a very narrow range of interparticle separation. The optimal condition is when neighboring particles are fully intercalated, namely, the interparticle separation was about one chainlength of the particle protecting ligands.<sup>2–4</sup> The fact that annealed particle dropcast films exhibit clear SET features implies that in comparison to the as-prepared particle film, drastic structural rearrangements of the nanoparticles occurred in the ensemble (as depicted in the lower inset to Fig. 2).

The structural evolution is further illustrated by the discrepancy of the temperature dependence of their film conductivity, as manifested in Fig. 3. First, it can be seen that except at  $320\ \text{K}$  where SET is prominent with the annealed film, the conductivity of the as-prepared film is somewhat higher than that of the annealed one throughout the temperature range of  $100$ – $310\ \text{K}$ . In addition, at low temperatures ( $<280\ \text{K}$ ), both films exhibit rather weak temperature dependence, suggesting that interparticle charge transfer might be primarily determined by tunneling between particles (patches) that are of equivalent energy states but not necessarily in close proximity. In contrast, at higher temperatures ( $>280\ \text{K}$ ), a clear Arrhenius profile can be seen, indicative of a thermal activation mechanism, and the activation energy ( $E_a$ ) of interparticle charge transfer can be found to increase from  $48\ \text{meV}$  for the as-prepared film to  $208\ \text{meV}$  after thermal annealing (the latter has been found to vary within  $100$ – $200\ \text{meV}$  with different particle concentrations and annealing temperatures, not shown). It should be noted that the activation energy of the as-prepared film is very close to those

found with dropcast films of nanoparticles of similar structures<sup>11</sup> and the  $E_a$  value of the annealed film is consistent with that of nanoparticle Langmuir–Blodgett monolayers that exhibit clear SET features.<sup>2–4</sup> As mentioned earlier, rampant structural defects within the as-prepared particle films lead to effective percolation pathways for interparticle charge transport, whereas after thermal annealing the energetic barrier to charge transfer increases because of the ordered arrangements of the nanoparticle cores in the organic matrix.

To better understand the molecular origin of the impacts of thermal annealing on nanoparticle conductivity properties, it should be noted that charge transfer in a nanoparticle solid is mainly governed by the three following factors: (i) dipolar coupling interactions between adjacent nanoparticles that define the overlap of electronic wave functions, (ii) disordered domains arising from particle structural dispersity and arrangements that may exhibit high impedance to interparticle charge transfer, and (iii) Coulombic repulsion of electrons on a given particle.<sup>16</sup> In other words, the interparticle charge transfer is highly dependent upon the arrangements of the nanoparticles (as well as the nanoparticle structures), which may be readily manipulated by temperature. It has been known that at increasing temperatures, nanoparticle solids undergo a clear phase transition, which has been manifested in differential scanning calorimetric and variable-temperature IR and NMR spectroscopic measurements.<sup>17–19</sup> For the AuC8 nanoparticles, the transition temperature is slightly lower than the ambient temperature.<sup>17</sup>

Therefore, two consequences are most likely to arise from thermal annealing even at a moderately elevated temperature, improved ordering of the nanoparticle (core) arrangements, and an increasing degree of conformational disordering of the organic matrix, thanks to the nanoparticle rotational and lateral mobility even in solid state. Their effects on nanoparticle film conductance may differ quite drastically. For instance, the formation of an ordered lattice of the nanoparticle cores may lead to enhancement of nanoparticle charge transfer because of the diminishment of the disordered domains; however, the embedment of the nanoparticle cores within the insulating organic matrix is anticipated to result in an increase of the energetic barrier for interparticle charge transfer, which may be further enhanced by the increasing conformational disordering of the organic matrix, because elevated temperatures favor gauche conformations of the protecting ligands and through-bond electron tunneling is much less efficient with the gauche conformation than with the trans counterpart.<sup>20</sup> On the basis of the experimental data shown above, it appears that the latter is more prominent than the former, leading to a decrease of the film conductivity and higher activation energy, as summarized in Fig. 3.

It should be mentioned that we have opted to keep the annealing temperature below 360 K out of concern of the stability of the IDA electrode as well as the nanoparticles. Within the present experimental context, thermal annealing is very effective in inducing discrete charge transfer with particle films of up to 100 layers, whereas for thicker films, the current-potential profiles remained featureless. This seems to imply that at these annealing temperatures, structural rearrangements are most probably limited to the particles close to the substrate surface where sufficient interparticle space was available. For thicker films, a higher annealing temperature is anticipated. In addition, for nanoparticles of different core size and surface protecting ligands, the optimal annealing temperature is likely to vary accordingly. These issues are being addressed in ongoing work and the results will be reported in due course.

This work was supported in part by the National Science Foundation (Grant Nos. CHE-0718190 and CHE-0832605). E.M. thanks the UCSC ACCESS program for a Summer Research Internship.

<sup>1</sup>S. W. Chen, R. S. Ingram, M. J. Hostetler, J. J. Pietron, R. W. Murray, T. G. Schaaff, J. T. Khoury, M. M. Alvarez, and R. L. Whetten, *Science* **280**, 2098 (1998).

<sup>2</sup>S. W. Chen, *J. Mater. Chem.* **17**, 4115 (2007).

<sup>3</sup>S. Pradhan, J. Sun, F. J. Deng, and S. W. Chen, *Adv. Mater. (Weinheim, Ger.)* **18**, 3279 (2006).

<sup>4</sup>Y. Y. Yang, S. Pradhan, and S. W. Chen, *J. Am. Chem. Soc.* **126**, 76 (2004).

<sup>5</sup>J. P. Choi, M. M. Coble, M. R. Branham, J. M. DeSimone, and R. W. Murray, *J. Phys. Chem. C* **111**, 3778 (2007).

<sup>6</sup>M. Brust, M. Walker, D. Bethell, D. J. Schiffrin, and R. Whyman, *J. Chem. Soc., Chem. Commun.*, 801 (1994).

<sup>7</sup>A. C. Templeton, M. P. Wuelfing, and R. W. Murray, *Acc. Chem. Res.* **33**, 27 (2000).

<sup>8</sup>S. W. Chen, *Langmuir* **17**, 6664 (2001).

<sup>9</sup>S. W. Chen, *Langmuir* **17**, 2878 (2001).

<sup>10</sup>M. J. Hostetler, J. E. Wingate, C. J. Zhong, J. E. Harris, R. W. Vachet, M. R. Clark, J. D. Londono, S. J. Green, J. J. Stokes, G. D. Wignall, G. L. Glish, M. D. Porter, N. D. Evans, and R. W. Murray, *Langmuir* **14**, 17 (1998).

<sup>11</sup>Y. Joseph, I. Besnard, M. Rosenberger, B. Guse, H. G. Nothofer, J. M. Wessels, U. Wild, A. Knop-Gericke, D. S. Su, R. Schlogl, A. Yasuda, and T. Vossmeier, *J. Phys. Chem. B* **107**, 7406 (2003).

<sup>12</sup>A. W. Snow and H. Wohltjen, *Chem. Mater.* **10**, 947 (1998).

<sup>13</sup>J. F. Sampaio, K. C. Beverly, and J. R. Heath, *J. Phys. Chem. B* **105**, 8797 (2001).

<sup>14</sup>D. Ghosh and S. W. Chen, *J. Mater. Chem.* **18**, 755 (2008).

<sup>15</sup>G. Schmid and U. Simon, *Chem. Commun. (Cambridge)*, 697 (2005).

<sup>16</sup>F. Remacle, *J. Phys. Chem. A* **104**, 4739 (2000).

<sup>17</sup>M. J. Hostetler and R. W. Murray, *Curr. Opin. Colloid Interface Sci.* **2**, 42 (1997).

<sup>18</sup>A. Badia, L. Cuccia, L. Demers, F. Morin, and R. B. Lennox, *J. Am. Chem. Soc.* **119**, 2682 (1997).

<sup>19</sup>A. Badia, S. Singh, L. Demers, L. Cuccia, G. R. Brown, and R. B. Lennox, *Chem.-Eur. J.* **2**, 359 (1996).

<sup>20</sup>M. Fujihira, M. Suzuki, S. Fujii, and A. Nishikawa, *Phys. Chem. Chem. Phys.* **8**, 3876 (2006).